IJMMM International Journal of Minerals, Metallurgy and Materials 矿物冶金与材料学报（英文版）

Hybrid model for BOF oxygen blowing time prediction based on oxygen balance mechanism and deep neural network

Xin Shao, Qing Liu, Zicheng Xin, Jiangshan Zhang, Tao Zhou, and Shaoshuai Li

Cite this article as:
Xin Shao, Qing Liu, Zicheng Xin, Jiangshan Zhang, Tao Zhou, and Shaoshuai Li, Hybrid model for BOF oxygen blowing time prediction based on oxygen balance mechanism and deep neural network, *Int. J. Miner. Metall. Mater.*, 31(2024), No. 1, pp. 106-117. https://doi.org/10.1007/s12613-023-2670-1

INTERNATIONAL JOURNAL OF
Minerals, Metallurgy and Materials

Volume 31, Number 1, January 2024
Page 106

Research Article https://doi.org/10.1007/s12613-023-2670-1

Hybrid model for BOF oxygen blowing time prediction based on oxygen balance mechanism and deep neural network

Xin Shao[1)], *Qing Liu*[1,2),✉], *Zicheng Xin*[1)], *Jiangshan Zhang*[1)], *Tao Zhou*[1)], *and Shaoshuai Li*[3)]

1) State Key Laboratory of Advanced Metallurgy, University of Science and Technology Beijing, Beijing 100083, China
2) Engineering Research Center of MES Technology for Iron & Steel Production, Ministry of Education, Beijing 100083, China
3) Laiwu Iron and Steel Group Yinshan Section Steel Co., Ltd., Jinan 271104, China
(Received: 23 February 2023; revised: 6 May 2023; accepted: 8 May 2023)

Abstract: The amount of oxygen blown into the converter is one of the key parameters for the control of the converter blowing process, which directly affects the tap-to-tap time of converter. In this study, a hybrid model based on oxygen balance mechanism (OBM) and deep neural network (DNN) was established for predicting oxygen blowing time in converter. A three-step method was utilized in the hybrid model. First, the oxygen consumption volume was predicted by the OBM model and DNN model, respectively. Second, a more accurate oxygen consumption volume was obtained by integrating the OBM model and DNN model. Finally, the converter oxygen blowing time was calculated according to the oxygen consumption volume and the oxygen supply intensity of each heat. The proposed hybrid model was verified using the actual data collected from an integrated steel plant in China, and compared with multiple linear regression model, OBM model, and neural network model including extreme learning machine, back propagation neural network, and DNN. The test results indicate that the hybrid model with a network structure of 3 hidden layer layers, 32-16-8 neurons per hidden layer, and 0.1 learning rate has the best prediction accuracy and stronger generalization ability compared with other models. The predicted hit ratio of oxygen consumption volume within the error ±300 m^3 is 96.67%; determination coefficient (R^2) and root mean square error (RMSE) are 0.6984 and 150.03 m^3, respectively. The oxygen blow time prediction hit ratio within the error ±0.6 min is 89.50%; R^2 and RMSE are 0.9486 and 0.3592 min, respectively. As a result, the proposed model can effectively predict the oxygen consumption volume and oxygen blowing time in the converter.

Keywords: basic oxygen furnace; oxygen consumption; oxygen blowing time; oxygen balance mechanism; deep neural network; hybrid model

1. Introduction

As the key section of the steel manufacturing process, the steelmaking–continuous casting process (SCCP) is a high-temperature reaction process (1500–1700°C) consisting of multiple processes, multiple physical-chemical reactions, and multiple phase changes [1–2]. Due to the characteristics of multi-process, multi-reaction, and quasi-continuous, SCCP has various uncertain factors that bring great challenges to production organization and scheduling. Therefore, realizing the efficient and stable production of SCCP is a hot issue that needs to be solved urgently for the green and intelligent transformation of the steel industry in recent years [3–4]. Uncertain events in the converter process, which are dominated by a fluctuation of the converter taping cycle, frequently damage the stable operation of the SCCP and hinder the improvement of production efficiency [5–6]. As the initial process, the converter disturbance will lead to the tense production rhythm of each process in SCCP, and then destroy the process production, such as causing the shutdown of process devices, reduction of casting speed, and stopping pouring in severe cases. It is a feasible method to solve such dynamic scheduling problems by predicting the possible uncertain factors through deeply analyzing the metallurgical reaction mechanism of SCCP [7].

For uncertain events in the production scheduling process, detecting disturbances in advance can achieve more efficient production scheduling [5]. Jiang *et al.* [8] developed a prediction-based online soft scheduling based on a surrogate model called Gaussian process regression to predict the characteristic index, slack ratio. Long *et al.* [9] established a release time series of hot metal ladles forecasting model using the historical data, and developed a new robust dynamic scheduling approach based on the release time series forecasting of molten iron ladle release. Yu *et al.* [10] deeply analyzed the relationship among operation time delay, planned casting break, and processing conflict, and then developed a novel prediction method for abnormal conditions of scheduling plan with operation time delay disturbance in SCCP, which reduces the frequency of complete rescheduling. Yang

✉ Corresponding author: Qing Liu E-mail: qliu@ustb.edu.cn

et al. [11] developed a new end-point temperature preset approach for molten steel in the final refining unit by integrating a deep neural network (DNN) and a multi-process operation simulation model, which solved the problem of the deviation between the actual casting temperature of molten steel and the preset temperature. In recent years, methods for predicting process parameters have been gradually applied to optimize the production scheduling of SCCP. However, SCCP is a complex physical and chemical reaction process, which leads to many unexpected production disturbances in the scheduling process, such as fluctuations in the smelting cycle, unsatisfactory composition, and unsatisfactory temperature of molten steel.

The converter smelting cycle is affected by the amount of oxygen blowing in the converter under the same smelting process. For the prediction of the amount of oxygen blowing, Cox *et al*. [12] used the probe to measure temperature and sample during the end-blow period and used these measurements as the inputs to the artificial neural networks model to predict how much oxygen to blow. Rajesh *et al*. [13] developed a multi-layered feed-forward neural network model for the prediction of end-blow oxygen in the converter, which was composed of a two-step process. Han and Zhao [14] proposed a dynamic control model based on an adaptive-network-based fuzzy inference system (ANFIS) and robust relevance vector machine to control the end-blow period of basic oxygen furnace (BOF), in which the ANFIS regression model was utilized to calculate the amounts of oxygen and coolant. Wang *et al*. [15] proposed a hybrid prediction model, based on twin support vector regression and whale optimization algorithm, which has high prediction accuracy. Ai *et al*. [16] used the Levenberg–Marquardt optimization algorithm to improve the back propagation neural network and established the prediction model of the total blow oxygen amount and the end blow oxygen amount in converter. Nowadays, prediction models based on various algorithms have been applied to predict the amount of oxygen blowing. Machine learning belongs to the black box model with strong adaptability but not strong interpretation of the converter metallurgical process. In contrast, the metallurgical mechanism model is a mathematical model that can describe the metallurgical process based on the analysis of the mass balance, energy balance, and chemical reactions. Dogan *et al*. [17] developed a comprehensive converter decarburization model to predict the carbon content of molten steel by investigating the decarburization mechanism in different reaction zones, which showed good agreement with plant data. The physical significance of the parameters in the mechanism model is clear, which makes the mechanism model have strong pertinence. Additionally, combining physical modelling with machine learning has a proven track record in various parameter prediction [18–20]. Therefore, it is necessary to introduce the metallurgical mechanism to predict the amount of oxygen blowing in the converter. Li *et al*. [21] considered the efficiency of oxygen decarburization and established a calculation model of blowing oxygen volume based on a support vector machine (SVM). Wang *et al*. [22] analyzed the converter oxygen balance and amalgamated it with a multiple linear regression (MLR) model to establish an integrated model for the prediction of the oxygen blowing quantity. Li *et al*. [21] and Wang *et al*. [22] considered the metallurgical mechanism in their research but made more simplifications to the converter reaction process, and there were problems with non-essential assumptions and incomplete consideration of influencing factors. In addition, SVM has insufficient ability to express large-scale high-dimensional data when dealing with complex nonlinear relationships and has the problem of difficult kernel function design and poor generalization ability. MLR shows a better fit when dealing with data with linear relationships, but it is difficult to approximate complex nonlinear relationships. DNN, as one of the hottest machine learning algorithms in recent years, relies on the multi-layer network structure to enable strong feature learning ability, good adaptability to nonlinear data relationships, and strong generalization ability [23–25]. Furthermore, different from process research which focuses on oxygen blowing volume, scheduling research pays more attention to the fluctuation of smelting time, because the production of each process ultimately affects the entire production scheduling in the form of time. Therefore, it is necessary to further predict the oxygen blowing time of the converter.

Aiming at the above problems, a hybrid model exploiting DNN and more comprehensive oxygen balance mechanism (OBM) was established for more accurate analysis of complex high-dimensional nonlinear data of the converter smelting process in this study. Based on the prediction of converter oxygen blowing volume, a converter oxygen blowing time prediction model was established to provide a reference for solving the fluctuation influence of converter taping cycle on the scheduling process. This work can establish a more accurate hybrid model to predict the oxygen blowing volume in converter and provide a novel technical idea for researchers in solving production scheduling problems.

2. Description and analysis of BOF process

2.1. Process description

Converter steelmaking is a batch process that uses a lance to blow oxygen into the converter furnace to convert rich-carbon hot metal into low-carbon molten steel. During the basic oxygen steelmaking process, the hot metal at about 1400°C is heated up to 1700°C mainly through carbon oxidation exotherm. During this period, the converter slag is made by adding lime dolomite in reasonable proportions, and the impurity elements such as carbon, silicon, manganese, and phosphorus are further removed by the stirring action of the oxygen jet, which finally converts the hot metal into molten steel.

The research object of this study is an integrated steel plant in China with an annual capacity of 5 Mt consisting of BOF, ladle furnace (LF), Ruhrstahl Heraeus (RH), and continuous casting (CC) processes. These are four converters in this plant. Each BOF loads about 120 t of hot metal and 20 t of scrap at a time and completes a smelting cycle in about 40 min. Approximately 29 heats are carried out every day.

The converter smelting process contains many operations, and the tap-to-tap of BOF is shown in Fig. 1, including scrap adding, hot metal charging, main blowing, sub-lance detection, end blowing, alloy addition, steel tapping, furnace shaking, slag splashing, and other operations.

The above operations can be divided into two categories, among which scrap adding, hot metal charging, sub-lance detection, furnace shaking, and slag splashing can be classified as management-related, and such operations can be greatly ensured to be on time through reasonable operating rules setting and strict operator training as well as regular maintenance of equipment. Another category of operations can be classified as process-related, such as main blowing and end blowing, which are physiochemically violent reaction process involving complex reaction thermodynamics and kinetics. Although the process-related operations account for a small proportion of the converter smelting cycle, the processing time of these operations is typically significantly variable due to the influence of the complex reaction mechanism and variation of smelting conditions in each heat. Therefore, it is of great significance to accurately predict the processing time of these operations for scheduling adjustment and production smoothness.

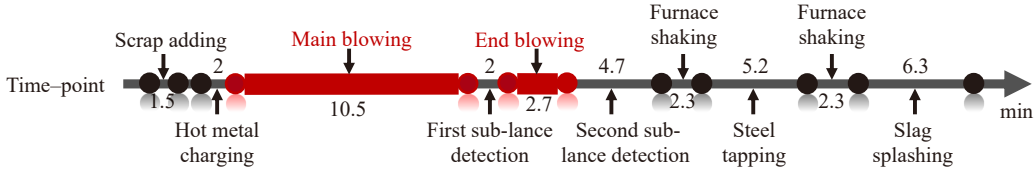

Fig. 1. Specific flow chart of converter smelting process.

2.2. Analysis of main factors

Under normal conditions, the converter oxygen blowing process is usually divided into two periods, namely the main blowing and the end blowing. The main blowing and end blowing are distinguished by the first temperature measurement and carbon determination of the sub-lance. During the blowing process, oxygen blowing will be paused usually when the blowing volume reaches about 85vol% of the total blowing volume [16,26]. Subsequently, the sub-lance is used for temperature measurement and carbon determination, and the oxygen blowing volume at the end blowing stage is calculated by comparing the measured carbon content with the expected value. Finally, the converter blowing is completed.

Hence, the whole blowing process is composed of main blowing, sub-lance detection, and end blowing. Since the process of sub-lance detection can be classified as a management-related problem, and a relatively definite detection time can be achieved through reasonable operation specifications and personnel training, this study ignores the sub-lance detection time and only considers the effect of blowing volume on the blowing time.

The converter blowing time is mainly influenced by the oxygen required volume, oxygen supply intensity, and the weight of molten steel, while the oxygen required volume is closely related to the elemental oxidation, oxygen decarburization efficiency, and the amount of oxygen brought in by the coolant. Based on the analysis of the BOF metallurgical reaction mechanism and literature survey [12–16,21–22,27–28], the main factors affecting the oxygen blowing time of BOF steelmaking were put forward. As shown in Table 1, the main variables include input variables related to element oxidation (X_1–X_8), input variables related to oxygen decarbonization efficiency (X_6–X_{12}), other related input variables (X_{13}–X_{14}), and output variables (Y_1–Y_2).

Table 1. Main factors affecting the oxygen blowing time of BOF steelmaking

Symbol	Description of variable	Unit	Symbol	Description of variable	Unit
X_1	Weight of hot metal	t	X_9	Temperature of hot metal	°C
X_2	Weight of scrap	t	X_{10}	Temperature of molten steel	°C
X_3	[C] content in molten steel	wt%	X_{11}	Weight of lime	t
X_4	[Si] content in molten steel	wt%	X_{12}	Weight of dolomite	t
X_5	[P] content in molten steel	wt%	X_{13}	Weight of sinter	t
X_6	[C] content in hot metal	wt%	X_{14}	Oxygen supply intensity	$m^3/(t \cdot min)$
X_7	[Si] content in hot metal	wt%	Y_1	Volume of oxygen	m^3
X_8	[P] content in hot metal	wt%	Y_2	Blowing time	min

3. Modelling in hybrid model

3.1. Deep neural network

The neural network was first proposed in 1943. On this basis, Hinton *et al*. [29] first introduced the concept of deep learning in 2006 and designed a DNN model containing seven hidden layers. The internal topology of the DNN, as shown in Fig. 2, consists of input layers, hidden layers, and output layers. When the number of hidden layers exceeds three and the hidden layers are fully connected to each other, it can be called DNN. The main feature of DNN that distinguishes it from other network structures (convolutional

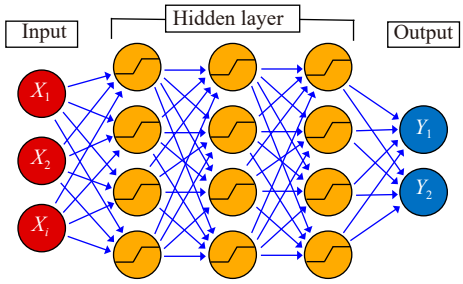

Fig. 2. Network topology structure of DNN.

neural network and recurrent neural network) is that the neurons of the previous layer are connected to the neurons of the latter layer [30–32].

The supervised learning process of DNN can be divided into two main steps. The first step is the training process, in which a topological neural network is established through hyperparameter settings. Further, the input data is fed to the DNN to determine appropriate values for node weights to solve a specific task during the iterative learning process. The second step is the inference process, which uses the trained model to make predictions on new data. In addition, the neural network has a strong nonlinear mapping ability because of the introduction of various activation functions in DNN, especially the rectified linear units (ReLU) which is a good solution to the gradient disappearance problem. Therefore, DNN has been widely used for the prediction of various process parameters in the steel industry. Liu *et al.* [33] proposed an integrated model based on a DNN and a long short-term memory (LSTM) network to help the field operators to control the change of the sinter composition in real time. Myers and Nakagaki [34] developed a DNN model to predict the nucleation lag time of iron and steelmaking melts solely from elemental composition and temperature, and achieved rapid design, analysis, and optimization of new slag compositions.

3.2. Oxygen balance mechanism

The converter steelmaking process is a complex high-temperature physical and chemical process. In this study, an OBM model for oxygen required prediction was established by analyzing the relevant chemical reactions and material balance.

In the converter smelting process, oxygen is injected into BOF by the oxygen lances, mainly for the oxidation of carbon and other elements. As a result, part of the oxygen element enters the converter dust and slag in the form of oxide, part of the oxygen element participates in the post-combustion of CO in the furnace, and part of the unused oxygen is discharged with the flue gas. In addition, some coolants such as sintered ore will bring in a certain amount of oxygen element.

Consequently, the income and expenditure of oxygen element in the converter smelting process can be summarized as shown in Fig. 3, and the oxygen balance equation is shown in Eq. (1).

$$V_{\text{O-blance}} = \sum m_i V_i + V_{\text{O-dust}} + V_{\text{O-slag}} + V_{\text{oxy-gas}} + V_{\text{O-CO}} - V_{\text{O-sinter}} \quad (1)$$

where $V_{\text{O-blance}}$ is the converter oxygen required volume, m^3;

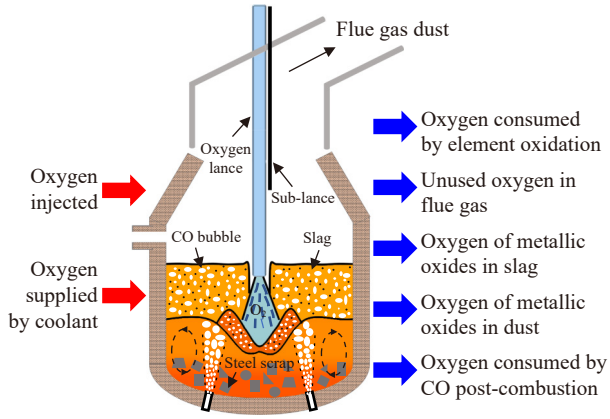

Fig. 3. Oxygen balance of BOF steelmaking process.

m_i is the oxidized mass of element i, including carbon, silicon, manganese, phosphorus, and sulfur, t; V_i is the oxygen consumption volume per unit mass of element i, m^3/t; $V_{\text{O-dust}}$, $V_{\text{O-slag}}$, $V_{\text{oxy-gas}}$, and $V_{\text{O-sinter}}$ are the oxygen volume in converter dust, slag, flue gas, and sinter ore; $V_{\text{O-CO}}$ is the oxygen consumption volume by post-combustion of CO, respectively, m^3.

The molten steel is heated by a large amount of heat released during the oxidation of element C, which is the main oxidizing element in the smelting process. The oxidation products of element C in the bath can be assumed that 90wt% of the carbon is oxidized to CO and 10wt% is oxidized to CO_2 [35]. The oxidation mass of carbon, silicon, manganese, phosphorus, and sulfur can be calculated by Eqs. (2)–(7), respectively, under the assumption that the total weight of the molten metal before and after smelting is constant.

$$m_{\text{C-CO}} = X_1 \times (X_6 - X_3) + X_2 \times (w_{\text{sC}} - X_3) \times 90\% \quad (2)$$

$$m_{\text{C-CO}_2} = X_1 \times (X_6 - X_3) + X_2 \times (w_{\text{sC}} - X_3) \times 10\% \quad (3)$$

$$m_{\text{Si}} = X_1 \times (X_7 - X_4) + X_2 \times (w_{\text{sSi}} - X_4) \quad (4)$$

$$m_{\text{Mn}} = X_1 \times (w_{\text{hMn}} - w_{\text{mMn}}) + X_2 \times (w_{\text{sMn}} - w_{\text{mMn}}) \quad (5)$$

$$m_{\text{P}} = X_1 \times (X_8 - X_5) + X_2 \times (w_{\text{sP}} - X_5) \quad (6)$$

$$m_{\text{S}} = X_1 \times (w_{\text{hS}} - w_{\text{mS}}) + X_2 \times (w_{\text{sS}} - w_{\text{mS}}) \quad (7)$$

where $m_{\text{C-CO}}$, $m_{\text{C-CO}_2}$, m_{Si}, m_{Mn}, m_{P}, and m_{S} are oxidation mass of C oxidized to CO, C oxidized to CO_2, Si, Mn, P, and S, respectively, t; w_{sC}, w_{sSi}, w_{sMn}, w_{sP}, and w_{sS} are the contents of C, Si, Mn, P, and S in scrap, respectively, wt%; w_{hMn} and w_{hS} are the contents of Mn and S in hot metal, respectively, wt%; w_{mMn} and w_{mS} are the contents of Mn and S in molten steel, respectively, wt%.

During the smelting process, oxygen in the dust and slag is mainly in the form of FeO and Fe_2O_3, the same as sinter ore. Therefore, the volume of oxygen in dust, slag, and sinter ore can be expressed by Eqs. (8)–(10), respectively.

$$V_{\text{O-dust}} = M_{\text{dust}} \cdot \left(C_{\text{FeO-dust}} \cdot \frac{16}{72} + C_{\text{Fe}_2\text{O}_3\text{-dust}} \cdot \frac{48}{160} \right) \cdot \frac{22.4}{32} \quad (8)$$

$$V_{\text{O-slag}} = M_{\text{slag}} \cdot \left(C_{\text{FeO-slag}} \cdot \frac{16}{72} + C_{\text{Fe}_2\text{O}_3\text{-slag}} \cdot \frac{48}{160} \right) \cdot \frac{22.4}{32} \quad (9)$$

$$V_{\text{O-sinter}} = M_{\text{sinter}} \cdot \left(C_{\text{FeO-sinter}} \cdot \frac{16}{72} + C_{\text{Fe}_2\text{O}_3\text{-sinter}} \cdot \frac{48}{160} \right) \cdot \frac{22.4}{32} \quad (10)$$

where M_{dust}, M_{slag}, and M_{sinter} are the mass of dust, slag, and sinter ore in each furnace, respectively, kg; C_{Feo-*} and $C_{Fe_2O_3-*}$ are the FeO and Fe_2O_3 content in * (*—dust, slag, and sinter ore), respectively, wt%.

According to the statistics of the studied steelmaking plants, the amount of dust was 1.16% of the weight of molten steel, and the dust contained 70wt% FeO and 20wt% Fe_2O_3. The sinter ore is used as a coolant in the converter smelting process. The content of FeO and Fe_2O_3 in the sinter ore was obtained from the composition test results of the corresponding batch and the amount of sinter ore added can be obtained directly from the production reports or calculated from the heat balance of the converter. In addition, in order to obtain the oxygen amount of iron oxides in the slag, it is necessary to establish the converter mass balance to solve for the slag mass and assume that the content of FeO and Fe_2O_3 in the slag is 9wt% and 3wt%, respectively, according to the expert experience system.

The amount of oxygen consumed by CO post-combustion is small and difficult to determine in the actual process, so it can be approximately ignored in the oxygen balance calculation. The oxygen blown into the converter contains a certain amount of impurity gas mainly nitrogen. Here, it is assumed that the impurity gas does not react with the molten steel, and all enter the flue gas. Therefore, it is also necessary to consider the volume of this part of the impurity gas when calculating the total oxygen blowing volume. So, the volume of free oxygen $V_{oxy-gas}$ in the flue gas and the volume of impurity gas Z can be solved from Eqs. (11)–(14) as follows. The final total volume of blown oxygen V_{oxygen} can be obtained by jointly solving Eqs. (11)–(14).

$$V_{gas} = V_{oxycarbide} + V_{oxysulfide} + V_{oxy-gas} + Z \tag{11}$$

$$V_{oxygen} = \sum m_i V_i + V_{O\text{-}dust} + V_{O\text{-}slag} + V_{O\text{-}CO} - V_{O\text{-}sinter} + V_{oxy-gas} + Z \tag{12}$$

$$V_{oxy-gas} = V_{gas} \cdot C_{oxy-gas} \tag{13}$$

$$Z = V_{oxygen} \cdot (1 - C_{oxygen}) \tag{14}$$

where V_{gas} is the total volume of flue gas, m^3; $V_{oxycarbide}$ and $V_{oxysulfide}$ are the volume of carbon oxide and sulfur oxide, m^3; V_{oxygen} is the total volume of oxygen blown in, m^3; $C_{oxy-gas}$ is the volume of free oxygen in the flue gas, vol%; C_{oxygen} is the oxygen purity, vol%.

3.3. Integration of DNN and OBM

In this study, a hybrid model was established based on the DNN model and the OBM model to improve the prediction accuracy of the oxygen blowing time in the converter. The production data of converter smelting process used to build the hybrid model were collected from the studied steelmaking plants in China. 80% of the data groups were randomly selected for training the hybrid model, and 20% of the data groups were used for model testing. Each data group consists of 16 variables (as described in Section 2.2). The number of variables in the DNN model directly affects the network size. Too many network nodes severely slow down the model convergence speed as more network nodes need to be tuned. Therefore, in order to minimize the number of tasks in the DNN training process and accelerate the training speed, the number of DNN variables needs to be reduced. Based on the analysis of the OBM, the element oxidation amount is the key influential factor of the oxygen required volume. For purpose of reducing the number of variables in the DNN model, the oxidation amount of major oxidized elements (C, Si, and P) and the steel temperature difference before and after smelting were obtained by comparing the hot metal with molten steel. In other words, the variables of X_3 and X_6, X_4 and X_7, X_5 and X_8, X_9 and X_{10} were merged into X_{15} (Δ[C]), X_{16} (Δ[Si]), X_{17} (Δ[P]), and X_{18} (ΔT), respectively. The structure diagram of the hybrid model is shown in Fig. 4. A three-step method was used to predict the oxygen blowing time in the converter.

Step 1: Oxygen required volume was predicted separately using the OBM model and the DNN model.

Step 2: A hybrid calculation expression was built based on the prediction results of the DNN model and the OBM model, as shown in Eq. (15).

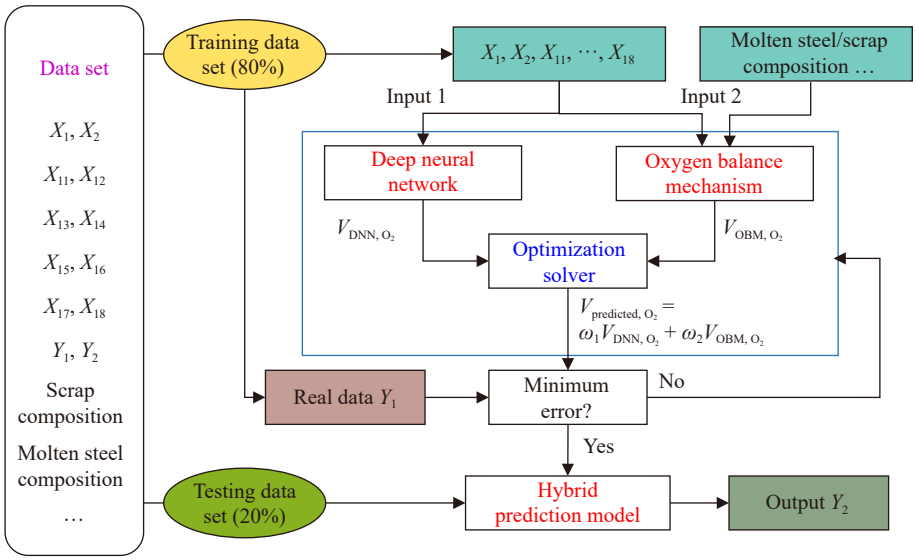

Fig. 4. Workflow of the hybrid model.

$$V_{\text{predicted},O_2} = \omega_1 \cdot V_{\text{DNN},O_2} + \omega_2 \cdot V_{\text{OBM},O_2} \quad (15)$$

where $V_{\text{predicted},O_2}$ is the predicted oxygen required volume, m^3; ω_1 and ω_2 are the weight coefficients of DNN model and OBM model, respectively; V_{DNN,O_2} and V_{DNN,O_2} are the prediction results of DNN model and OBM model, respectively.

Step 3: The BOF blowing time was calculated according to the optimized oxygen required volume with the oxygen supply intensity based on the test data set as shown in Eq. (16).

$$t_{\text{blowing}} = \frac{V_{\text{predicted},O_2}}{W \cdot I} \quad (16)$$

where t_{blowing} is the BOF total blowing time, min; W is the weight of molten steel, t; I is the oxygen supply intensity, $m^3/(t \cdot min)$.

Since the weight coefficients play an important role in the prediction accuracy of the model, Matlab was used to optimize the solution of Eq. (15) to determine the optimal weight coefficients for the DNN model and the OBM model. The objective function is established as shown in Eq. (17).

$$f = \min \sum_{i=1}^{n} \left| V_{\text{measured},O_2} - (\omega_1 \cdot V_{\text{DNN},O_2} + \omega_2 \cdot V_{\text{OBM},O_2}) \right|$$
$$\text{Subject to: } \omega_1 + \omega_2 = 1,\ \omega_1 > 0,\ \omega_2 > 0 \quad (17)$$

where V_{measured,O_2} is the actual oxygen consumption volume, m^3.

4. Modelling in hybrid model

4.1. Data cleaning

The original data set offered by the studied steelmaking plants was analyzed using a boxplot to remove outliers. As shown in Fig. 5(a), the boxplot uses quartiles to partition the data set. The quartiles are the three data points that divide the data set sorted by value into four groups in quantity, which are noted as quartile ($Q1$), median ($Q2$), and upper quartile ($Q3$). Among them, the difference between $Q3$ and $Q1$ is called the interquartile range (IQR). A smaller IQR means that the data in the middle part are more concentrated; a larger IQR means that the data in the middle part are more scattered. The outliers of the data set are defined as being above the upper limit ($Q3$ + 1.5IQR) or below the lower limit ($Q1$ − 1.5IQR). Fig. 5(b) shows the boxplot of the original data set for each variable after normalization, and the statistical description of each variable after removing outliers is shown in Table 2. The mathematical formula for the normalization process is shown in Eq. (18).

$$x' = \frac{x - \text{Min}}{\text{Max} - \text{Min}} \quad (18)$$

where x and x' are the values before and after conversion respectively; Max and Min are the maximum and minimum values of the sample, respectively.

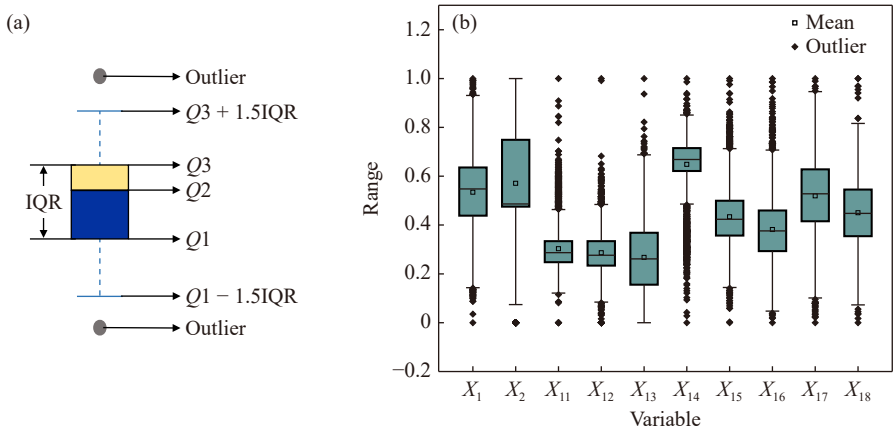

Fig. 5. Data cleaning by boxplot: (a) structure of the boxplot; (b) original data outlier detection based on boxplot.

Table 2. Descriptive statistics of variables after data cleaning

Symbol	Description of variable	Unit	Mean	Max	Min	Standard deviation
X_1	Weight of hot metal	t	127.16	144.70	109.30	6.68
X_2	Weight of scrap	t	15.98	27.42	2.04	4.98
X_{11}	Weight of lime	t	4.60	7.45	1.96	0.90
X_{12}	Weight of dolomite	t	2.15	3.65	0.65	0.55
X_{13}	Weight of sinter	t	3.20	8.31	0.20	1.62
X_{14}	Oxygen supply intensity	$m^3/(t \cdot min)$	2.95	3.34	2.66	0.12
X_{15}	Δ[C]	wt%	4.4146	4.7889	4.0323	0.1402
X_{16}	Δ[Si]	wt%	0.4239	0.7278	0.1287	0.1095
X_{17}	Δ[P]	wt%	0.1201	0.1533	0.0877	0.0116
X_{18}	ΔT	°C	359.18	465	252	38.44
Y_1	Volume of oxygen	m^3	6588.82	7356	5869	267.25
Y_2	Blowing time	min	15.68	29.20	12.95	1.55

There are 3128 groups of data retained after data cleaning with the boxplot, of which 2528 groups (about 80%) will be used for subsequent model training and 600 groups (about 20%) will be used for model testing. It can be known from Table 2 that the weight of the hot metal, scrap, lime, dolomite, and sinter was in the range of 109.30–144.70 t, 2.04–27.42 t, 1.96–7.45 t, 0.65–3.65 t, and 0.20–8.31 t, respectively. The value of oxygen supply intensity was 2.66 to 3.34 $m^3 \cdot t^{-1} \cdot min^{-1}$. The range of [C], [Si], and [P] variation value was 4.0323wt%–4.7889wt%, 0.1287wt%–0.7278wt%, and 0.0877wt%–0.1533wt%, respectively. The value of temperature variation ranged from 252 to 465°C. In addition, the average oxygen consumption was 6588.82 m^3, and the average oxygen blowing time was 15.68 min.

4.2. Correlation analysis

Correlation analysis was performed on the 9 input variables used in the DNN model to predict oxygen consumption volume (Y_1). The correlations between the different variables were statistically analyzed by Pearson correlation coefficient (r) and its significance testing based on the student's t-test (t). The calculation methods are shown in Eqs. (19)–(20). The results of the correlation analysis between the different variables are shown in Fig. 6 and Table 3.

$$r = \frac{\sum_{i=1}^{n}(x_i - \bar{x})(y_i - \bar{y})}{\sqrt{\sum_{i=1}^{n}(x_i - \bar{x})^2 \sum_{i=1}^{n}(y_i - \bar{y})^2}} \tag{19}$$

$$t = \frac{r\sqrt{n-2}}{\sqrt{1-r^2}} \tag{20}$$

where n is the sample size of the variable; x_i and y_i are the ith value of the input variable and output variable for all data points, respectively; $\bar{x}$ and $\bar{y}$ are the mean value of the input variable and output variable for all data points, respectively.

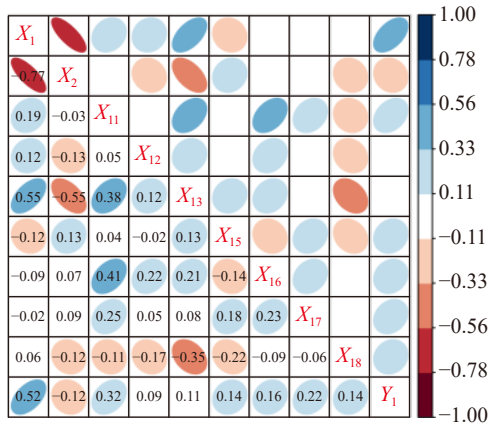

Fig. 6. Heatmap of Pearson correlation coefficient.

Table 3. Results of significance testing between Y_1 and the input variables

Variable	r	p-value	Variable	r	p-value
X_1	0.52	5.02×10^{-214}**	X_{15}	0.14	5.99×10^{-16}**
X_2	−0.12	2.84×10^{-12}**	X_{16}	0.16	6.76×10^{-19}**
X_{11}	0.32	1.25×10^{-76}**	X_{17}	0.22	4.06×10^{-36}**
X_{12}	0.09	7.44×10^{-7}**	X_{18}	0.14	3.06×10^{-14}**
X_{13}	0.11	8.09×10^{-10}**			

In Fig. 6, red represents positive correlation and blue represents negative correlation. The correlation gradually increases with the deepening of color and the decrease of color area. From the figure, it can be seen that there is a strong correlation between the input variables and the volume of oxygen (Y_1), except for the weight of dolomite (X_{12}) and the weight of sinter (X_{13}). Although the correlation between the weight of dolomite (X_{12}) and the weight of sinter (X_{13}) with the volume of oxygen (Y_1) is weak, in fact, dolomite is an important addition material in slagging, which affects the oxidation reaction of the element during the converter process. Moreover, sinter ore, as an important coolant, will transfer a proportion of oxygen element to the molten steel after being added. Hence, both are not negligible for predicting the volume of oxygen blowing.

In order to test the significance of the correlation coefficient between two variables, the p-value was employed. Usually, the correlation between the two variables is considered significant when the p-value is less than 0.05, and highly significant when the p-value is less than 0.01. As can be seen from Table 3, the p-values between the volume of oxygen (Y_1) and all input variables are less than 0.01, reaching a very significant correlation, and can be identified as input variables for the DNN model.

4.3. Model evaluation

In this study, determination coefficient (R^2) and root mean square error (RMSE) were employed to evaluate the performance of various models. The mathematical expressions of R^2 and RMSE are displayed in Eqs. (21)–(22). R^2 indicates the goodness of fit of the model. The larger R^2 represents the higher degree of explanation of the dependent variable by the independent variable. RMSE is a measure of the difference between the predicted and true values of a model. When the prediction hit ratio of two models is same, the smaller RMSE represents a higher prediction stability. Therefore, the larger R^2, the better the model performance, whereas the smaller RMSE, the better the model performance.

$$R^2 = 1 - \frac{\sum_{i=1}^{m}\left(y_i^{\text{act}} - y_i^{\text{pre}}\right)^2}{\sum_{i=1}^{m}\left(y_i^{\text{act}} - \overline{y_i^{\text{act}}}\right)^2} \tag{21}$$

$$\text{RMSE} = \sqrt{\frac{1}{m}\sum_{i=1}^{m}\left(y_i^{\text{act}} - y_i^{\text{pre}}\right)^2} \tag{22}$$

where y_i^{act} is the actual data; y_i^{pre} is the predicted value; $\overline{y_i^{act}}$ is the mean of actual data; m is the number of the total data set.

5. Results and discussion

5.1. Hyperparameter optimization of DNN model

The DNN model and the OBM model work together to determine the performance of the hybrid model. The OBM model created a fixed calculation procedure by establishing mathematical relationships within each data group, which makes the data group independent of each other. As a result, establishing a high-efficient DNN model is crucial for the hybrid model.

DNN is a specific network topology that contains one or more hidden layers. Hyperparameter settings such as the number of hidden layers, the number of neurons, the activation function, the learning rate, and the number of iterations have a significant impact on the learning ability of DNNs. Extremely strong learning ability can be achieved by reasonable hyperparameter settings, so this section focuses on optimizing the hyperparameter settings of the DNN model.

Activation functions are a class of nonlinear functions that map the input of a neuron to the output, which play an indispensable role in improving the learning ability of the neural network. The application of the activation functions avoids the linear transfer between the input and output of the hidden layer and increases the nonlinearity of the neural network. This change allows the neural network to approximate arbitrary nonlinear functions and greatly enhances the ability of the neural network to learn complex data.

The activation functions can be divided into two main categories: saturated activation functions represented by sigmoid and hyperbolic tangent (tanh); unsaturated activation functions represented by ReLU. Compared with the saturated activation function, the unsaturated activation function can effectively solve the gradient disappearance problem of neural networks and converge faster, so ReLU has become the most commonly used activation function for deep learning at present.

In this study, ReLU and bayesian regularization (trainbr) were chosen as the activation function and training function, respectively. Considering the training size, the optional range of the hyperparameters has been limited, as shown in Table 4, along with the initialized values of the hyperparameters. Hidden layers' number, neurons number of hidden layer, and learning rate were sequentially optimized. Moreover, according to the study in Ref. [34], the ratio of the neuron numbers in the next and previous hidden layers was set to 0.5 in further training. Each hyperparameter set was run 50 times. The average of RMSE was chosen as the indicator to evaluate the performances of each hyperparameter set. Fig. 7(a)–(c) shows the RMSE of each hyperparameter set, and the distribution of the final predicted value of oxygen consumption volume is shown in Fig. 7(d). The actual value in the figure

Table 4. Initialization hyperparameter setting of neural networks

Item	Initialized value	Range
Number of hidden layers	3	1–6
Neurons number of hidden layer	8	8–64
Learning rate	0.1	0.01–0.5

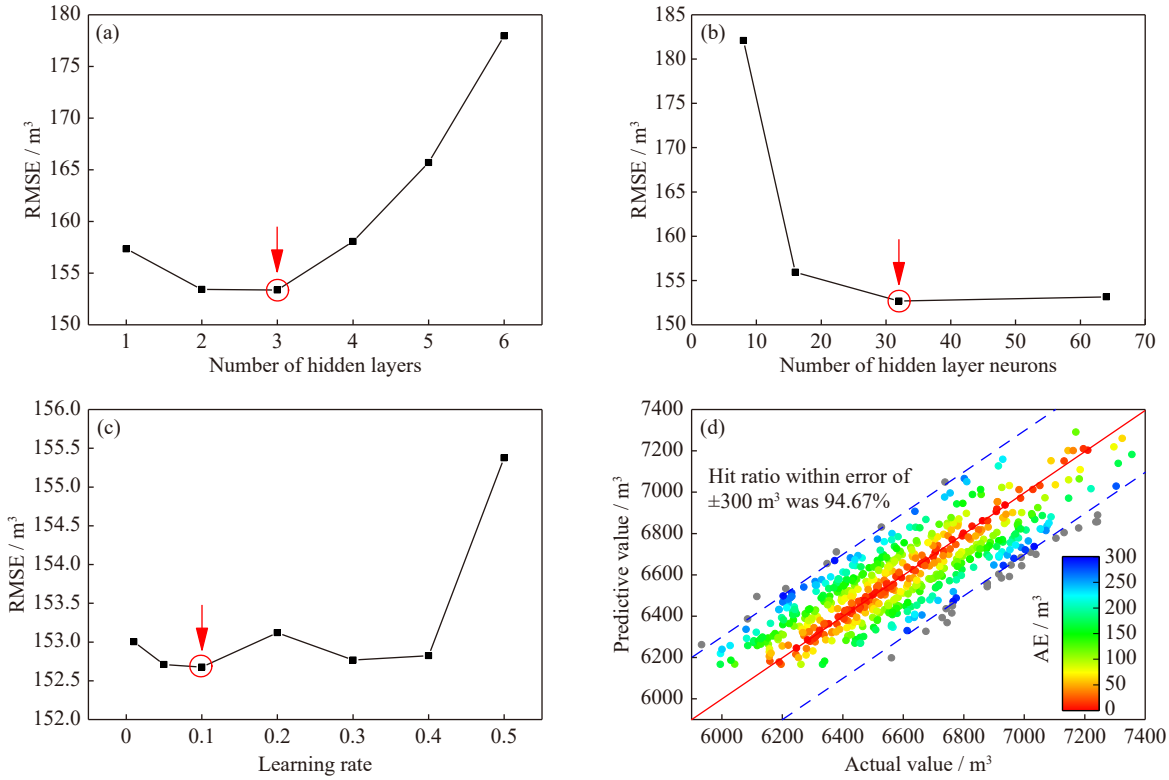

Fig. 7. Values of RMSE with the increments of (a) the number of hidden layers, (b) the number of hidden layer neurons, and (c) the learning rate as well as (d) the distribution of predicted values obtained by DNN model.

refers to the actual data from the testing dataset, while the predictive value represents the results obtained by the DNN model. The color scale in the lower right corner shows the absolute error (AE) value corresponding to each color, and the AE between the actual value and the predicted value of each data point was distinguished by different colors.

It is universally acknowledged that the smaller the RMSE, the better the performance of the model. Thus, the optimal DNN model hyperparameters are the hidden layer (3), the number of hidden layer neurons (32-16-8), and the learning rate (0.1), which can be seen in Fig. 7(a)–(c). Based on the above hyperparameter settings, the test results of the optimized DNN model are shown in Fig. 7(d), with the hit ratio within the error ±300 m^3 (relative error less than 5%) of 94.67%, R^2 of 0.6874, and RMSE of 152.74 m^3.

5.2. Comparison of application results

The hybrid model can be constructed by integrating the DNN model with the OBM model according to the method described in Section 3.3. By solving Eq. (15) through Matlab, we obtain the values of weight coefficients ω_1 and ω_2 for DNN model and OBM model as 0.81 and 0.19, respectively. The prediction results of the hybrid model based on DNN and OBM models are shown in Fig. 8. Similar to Fig. 7, the actual value and predictive value in Fig. 8 are the data from testing dataset and the results predicted by the hybrid model, respectively. The predicted hit ratio of oxygen consumption volume within the error ±300 m^3 is 96.67%, R^2 is 0.6984, and RMSE is 150.03 m^3. The oxygen blow time prediction hit ratio within the error ±0.6 min is 89.50%, R^2 is 0.9486, and RMSE is 0.3592 min.

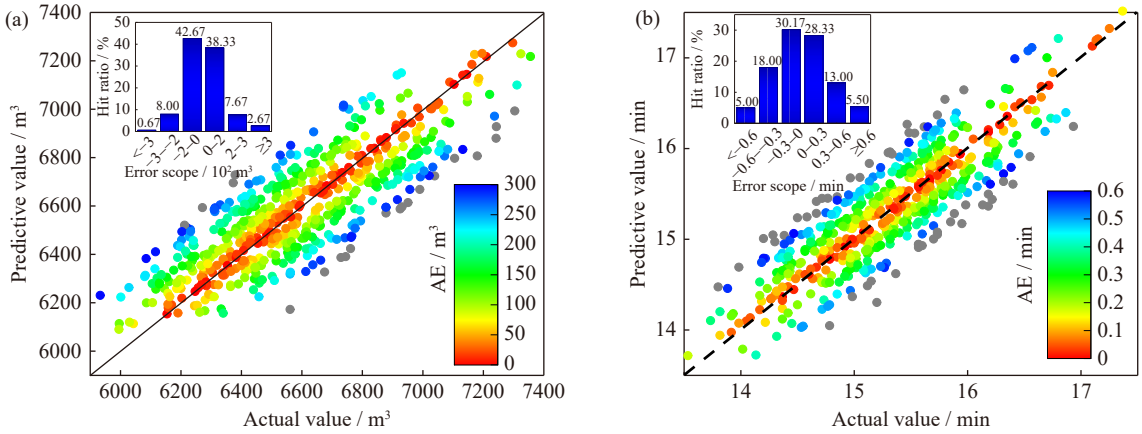

Fig. 8. Comparison of actual value and prediction value obtained by hybrid model: (a) the oxygen consumption volume; (b) the oxygen blow time. The upper left corner of the (a) and (b) presents the hit ratio statistics of the oxygen consumption volume and the oxygen blow time within different error ranges, respectively.

Furthermore, in order to better evaluate the hybrid model proposed in this study, extreme learning machine (ELM) model, DNN model, OBM model, multiple linear regression (MLR) model, and back propagation (BP) neural network model were also constructed for predicting the oxygen consumption volume and comparing the model performance with that of the hybrid model. The error distribution of the predicted oxygen consumption volume and the values of model evaluation indicators (hit ratio, R^2, and RMSE) for each model are shown in Fig. 9.

It is not hard to observe from Fig. 9 that the order of model performance from best to inferior is hybrid model, DNN, BP, ELM, MLR, and OBM. The MLR model has the characteristics of fast modelling speed and fast solution speed under mass data. However, as a linear model, the MLR model is difficult to deal with the interaction effect and nonlinear causality between variables when solving nonlinear problems, which leads to poor fitting [36]. In contrast, DNN, BP, and ELM, as neural network models, use nonlinear activation functions to transmit data between different network layers. Data features can be stored through neural units to achieve excellent learning ability when dealing with nonlinear problems. Therefore, the prediction hit ratio of neural network models such as DNN, BP, and ELM is higher than that of MLR model.

In addition, compared with shallow neural network (SNN) models such as BP and ELM, there are more hidden layers and neurons in the DNN model. This change endows the DNN model with stronger data processing ability and more complex nonlinear mapping relationship, which once again strengthens the learning ability of neural networks [37–38]. When using DNN to deal with the complex high-dimensional nonlinear data of converter smelting process, the neurons in the latter hidden layer of the DNN will perform linear operations on the input signals from all the neurons in the previous hidden layer, and then use the activation function to perform nonlinear processing on the linear operation results to generate new output signals, which are propagated backward layer by layer to the output layer. At the same time, the output loss of training samples is evaluated by the loss function, which ensures that the model output of all training samples is equal to or close to the true output of the sample as much as possible. Thus, the prediction hit ratio of DNN model is higher than that of SNN models, and has better generalization ability in this test.

The hybrid model proposed in this paper adds the mech-

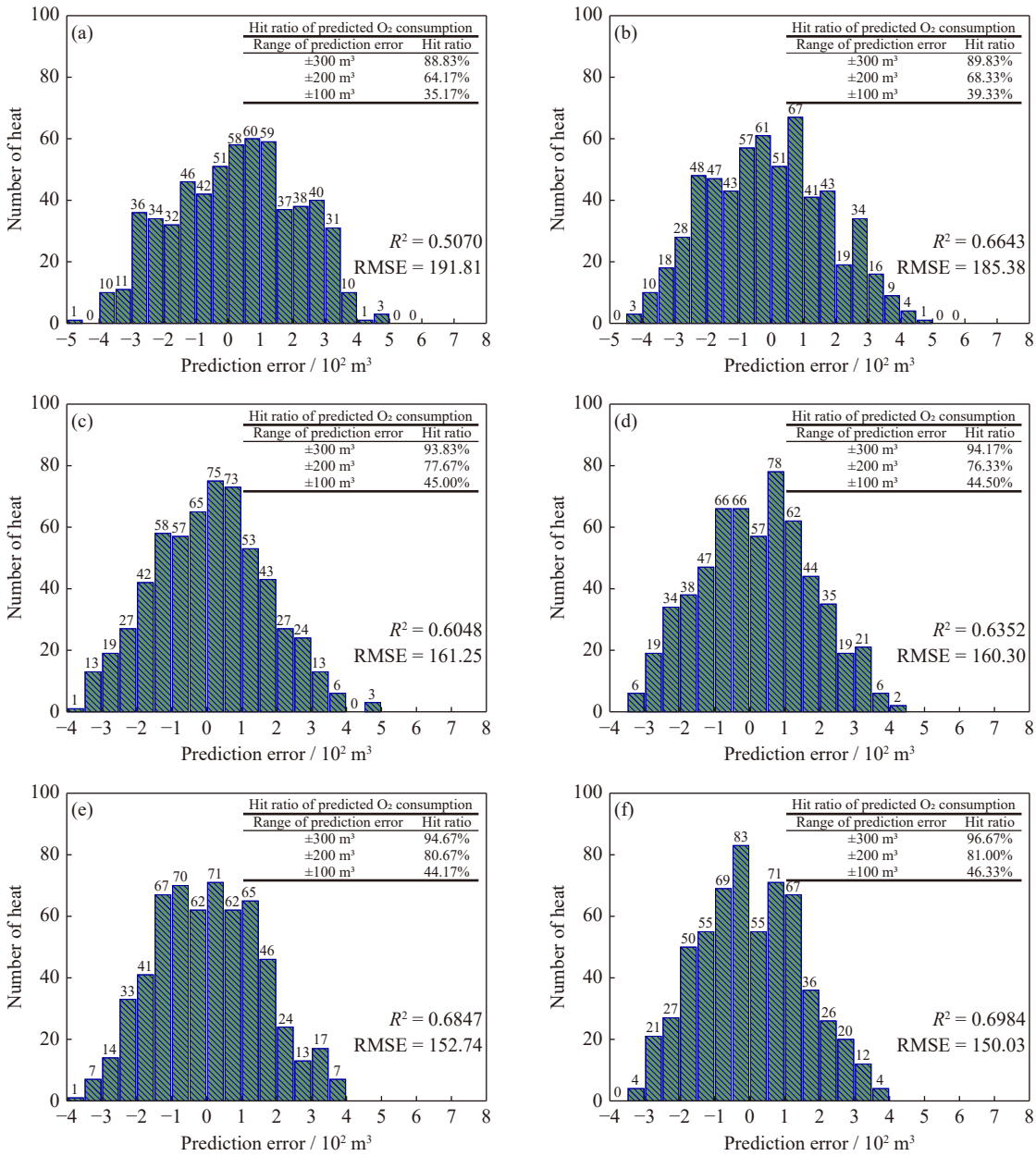

Fig. 9. Distribution of prediction error and hit ratio of different models: (a) OBM, (b) MLR, (c) ELM, (d) BP, (e) DNN, and (f) hybrid model.

anistic model on the basis of DNN model, which not only maintains the advantages of the DNN model, but also enhances the description and explanation of the complex reaction process of converter metallurgy based on the OBM. As shown in the results, the hybrid model has the best model performance compared to other models in terms of prediction hit ratio, determination coefficient, and root mean square error.

6. Conclusions

In this study, a hybrid model based on DNN and OBM models has been constructed for predicting the oxygen blowing time in the converter smelting process, and the following conclusions can be obtained.

(1) Based on the metallurgical mechanism of converter, an OBM model was constructed and a total of 14 variables affecting the oxygen consumption volume and oxygen blowing time were obtained that could be classified into three categories. They are element oxidation related (X_1–X_8), oxygen decarbonization efficiency related (X_6–X_{12}), and other related (X_{13}–X_{14}).

(2) Optimal DNN model hyperparameters have been found. Within the defined hyperparameter range, the optimal network structure of the DNN model is as follows: 3 hidden layer layers, 32-16-8 neurons per hidden layer, and 0.1 learning rate. A hybrid model based on the DNN and OBM models was established by a three-step method, and the weight coefficients of the DNN model and OBM model were determined to be 0.81 and 0.19, respectively.

(3) Five models of DNN, BP, ELM, MLR, and OBM with three evaluation indicators of hit ratio, R^2, and RMSE are em-

ployed for model performance validation. The results demonstrate that the model performance of the hybrid model established in this study is better than the other five models. In the error scope from −300 to 300 m^3, the hit ratio of oxygen consumption volume was 96.67%, and the R^2 and RMSE were 0.6984 and 150.03 m^3, respectively. Meanwhile, in the error scope from −0.6 to 0.6 min, the oxygen blow time hit ratio of hybrid model was 89.50%, and the R^2 and RMSE were 0.9486 and 0.3592 min, respectively.

(4) The hybrid model established in this study has higher prediction accuracy and generalization ability to predict the oxygen consumption volume and oxygen blowing time in the converter smelting process. The time deviation between the actual smelting cycle and the planned smelting cycle can be known in advance, which will greatly help to solve the dynamic scheduling problem.

Acknowledgements

This work was financially supported by the National Natural Science Foundation of China (Nos. 51974023 and 52374321) and the funding of State Key Laboratory of Advanced Metallurgy, University of Science and Technology Beijing, China (No. 41620007).

Conflict of Interest

The manuscript has not been published before and is not being considered for publication elsewhere. All authors have contributed to this manuscript for important intellectual content and review and approved the final manuscript. The authors declare no potential conflict of interest.

References

[1] R.Y. Yin, *Theory and Method of Metallurgical Process Integration*, 1st ed., Metallurgical Industry Press, Beijing, 2016, p. 102.

[2] Q. Liu, X. Shao, J.P. Yang, and J.S. Zhang, Multiscale modeling and collaborative manufacturing for steelmaking plants, *Chin. J. Eng*, 43(2021), No. 12, p. 1698.

[3] R.Y. Yin, Review on the study of metallurgical process engineering, *Int. J. Miner. Metall. Mater.*, 28(2021), No. 8, p. 1253.

[4] Z.J. Xu, Z. Zheng, and X.Q. Gao, Operation optimization of the steel manufacturing process: A brief review, *Int. J. Miner. Metall. Mater.*, 28(2021), No. 8, p. 1274.

[5] M. Iglesias-Escudero, J. Villanueva-Balsera, F. Ortega-Fernandez, and V. Rodriguez-Montequín, Planning and scheduling with uncertainty in the steel sector: A review, *Appl. Sci.*, 9(2019), No. 13, art. No. 2692.

[6] D. García-Menéndez, H. Morán-Palacios, F. Ortega-Fernández, and M. Díaz-Piloñeta, Scheduling in continuous steelmaking casting: A systematic review, *ISIJ Int.*, 60(2020), No. 6, p. 1097.

[7] Q. Liu, Q. Liu, J.P. Yang, *et al*., Progress of research on steelmaking-continuous casting production scheduling, *Chin. J. Eng.*, 42(2020), No. 2, p. 144.

[8] S.L. Jiang, M. Liu, J.H. Lin, and H.X. Zhong, A prediction-based online soft scheduling algorithm for the real-world steelmaking-continuous casting production, *Knowl. Based Syst.*, 111(2016), p. 159.

[9] J.Y. Long, Z.Z. Sun, P.M. Pardalos, Y. Bai, S.H. Zhang, and C. Li, A robust dynamic scheduling approach based on release time series forecasting for the steelmaking-continuous casting production, *Appl. Soft Comput.*, 92(2020), art. No. 106271.

[10] S.P. Yu, A prediction method for abnormal condition of scheduling plan with operation time delay in steelmaking and continuous casting production process, *ISIJ Int.*, 53(2013), No. 6, p. 1028.

[11] J.P. Yang, J.S. Zhang, W.D. Guo, S. Gao, and Q. Liu, End-point temperature preset of molten steel in the final refining unit based on an integration of deep neural network and multi-process operation simulation, *ISIJ Int.*, 61(2021), No. 7, p. 2100.

[12] I.J. Cox, R.W. Lewis, R.S. Ransing, H. Laszczewski, and G. Berni, Application of neural computing in basic oxygen steelmaking, *J. Mater. Process. Technol.*, 120(2002), No. 1-3, p. 310.

[13] N. Rajesh, M.R. Khare, and S.K. Pabi, Feed forward neural network for prediction of end-blow oxygen in LD converter steel making, *Mater. Res.*, 13(2010), No. 1, p. 15.

[14] M. Han and Y. Zhao, Dynamic control model of BOF steelmaking process based on ANFIS and robust relevance vector machine, *Expert Syst. Appl.*, 38(2011), No. 12, p. 14786.

[15] M. Wang, C. Gao, X.G. Ai, B.P. Zhai, and S.L. Li, Hybrid end-point static control model for 80 tons BOF steelmaking, *Trans. Indian Inst. Met.*, 75(2022), No. 9, p. 2281.

[16] X.L. Ai, Y.S. Wang, and W.M. Tang, Prediction of oxyen blow rate in BP neural network based converter refining, *Steelmaking*, 29(2013), No. 2, p. 34.

[17] N. Dogan, G.A. Brooks, and M.A. Rhamdhani, Comprehensive model of oxygen steelmaking part 1: Model development and validation, *ISIJ Int.*, 51(2011), No. 7, p. 1086.

[18] C.G. Shen, C.C. Wang, X.L. Wei, Y. Li, S. van der Zwaag, and W. Xu, Physical metallurgy-guided machine learning and artificial intelligent design of ultrahigh-strength stainless steel, *Acta Mater.*, 179(2019), p. 201.

[19] W.Z. Mu, M. Rahaman, F.L. Rios, J. Odqvist, and P. Hedström, Predicting strain-induced martensite in austenitic steels by combining physical modelling and machine learning, *Mater. Des.*, 197(2021), art. No. 109199.

[20] Z.C. Xin, J.S. Zhang, J.G. Zhang, J. Zheng, Y. Jin, and Q. Liu, Predicting temperature of molten steel in LF-refining process using IF-ZCA-DNN model, *Metall. Mater. Trans. B*, 54(2023), No. 3, p. 1181.

[21] Y. Li, M. Han, and L.W. Jiang, Blowing oxygen volume calculation model of BOF steelmaking based on oxygen decarburization efficiency prediction, *J. Dalian Univ. Technol.*, 52(2012), No. 5, p. 725.

[22] Z. Wang, Q. Liu, F.M. Xie, *et al*., Model for prediction of oxygen required in BOF steelmaking, *Ironmaking Steelmaking*, 39(2012), No. 3, p. 228.

[23] S.W. Wu, J. Yang, and G.M. Cao, Prediction of the Charpy V-notch impact energy of low carbon steel using a shallow neural network and deep learning, *Int. J. Miner. Metall. Mater.*, 28(2021), No. 8, p. 1309.

[24] I. Mohanty, R. Banerjee, A. Santara, S. Kundu, and P. Mitra, Prediction of properties over the length of the coil during thermo-mechanical processing using DNN, *Ironmaking Steelmaking*, 48(2021), No. 8, p. 953.

[25] S. Mittal, A survey on modeling and improving reliability of DNN algorithms and accelerators, *J. Syst. Archit.*, 104(2020), art. No. 101689.

[26] F. He, X.Y. Chai, and Z.H. Zhu, Prediction of oxygen-blowing volume in BOF steelmaking process based on BP neural network and incremental learning, *High Temp. Mater. Process.*, 41(2022), No. 1, p. 403.

[27] W.H. Lin, S.Q. Jiao, J.K. Sun, M. Liu, X. Su, and Q. Liu, Modified exponential model for carbon prediction in the end blow-

ing stage of basic oxygen furnace converter, *Chin. J. Eng.*, 42(2020), No. 7, p. 854.
[28] G.H. Li, B. Wang, Q. Liu, *et al*., A process model for BOF process based on bath mixing degree, *Int. J. Miner. Metall. Mater.*, 17(2010), No. 6, p. 715.
[29] G.E. Hinton, S. Osindero, and Y.W. Teh, A fast learning algorithm for deep belief nets, *Neural Comput.*, 18(2006), No. 7, p. 1527.
[30] Y. Bengio, *Learning Deep Architectures for AI*, Now Foundations and Trends, Boston, 2009, p. 44.
[31] S. Shamshirband, M. Fathi, A. Dehzangi, A.T. Chronopoulos, and H. Alinejad-Rokny, A review on deep learning approaches in healthcare systems: Taxonomies, challenges, and open issues, *J. Biomed. Inform.*, 113(2021), art. No. 103627.
[32] Y.G. Zhang, Y.L. Xie, Y. Zhang, J.B. Qiu, and S.X. Wu, The adoption of deep neural network (DNN) to the prediction of soil liquefaction based on shear wave velocity, *Bull. Eng. Geol. Environ.*, 80(2021), No. 6, p. 5053.
[33] S. Liu, X.J. Liu, Q. Lyu, and F.M. Li, Comprehensive system based on a DNN and LSTM for predicting sinter composition, *Appl. Soft Comput.*, 95(2020), art. No. 106574.
[34] C.A. Myers and T. Nakagaki, Prediction of nucleation lag time from elemental composition and temperature for iron and steelmaking slags using deep neural networks, *ISIJ Int.*, 59(2019), No. 4, p. 687.
[35] R.J. Fruehan, *The Making, Shaping and Treating of Steel: Steelmaking and Refining Volume*, 11th ed., The AISE Steel Foundation, Pittsburgh, 1998, p. 496.
[36] Z.C. Xin, J.S. Zhang, J. Zheng, Y. Jin, and Q. Liu, A hybrid modeling method based on expert control and deep neural network for temperature prediction of molten steel in LF, *ISIJ Int.*, 62(2022), No. 3, p. 532.
[37] J. Schmidhuber, Deep learning in neural networks: An overview, *Neural Netw.*, 61(2015), p. 85.
[38] Y. LeCun, Y. Bengio, and G. Hinton, Deep learning, *Nature*, 521(2015), No. 7553, p. 436.